

## Research Article

# Remote Sensing Image Water Body Recognition Algorithm Based on Deep Convolution Generating Network and Combined Features

Yan Zhao  and Caiying Feng

College of Information and Electronic Engineering, Shangqiu Institute of Technology, Shangqiu 476000, China

Correspondence should be addressed to Yan Zhao; 1350007050@sqgxy.edu.cn

Received 31 March 2022; Revised 9 May 2022; Accepted 20 May 2022; Published 16 June 2022

Academic Editor: Zhiguo Qu

Copyright © 2022 Yan Zhao and Caiying Feng. This is an open access article distributed under the Creative Commons Attribution License, which permits unrestricted use, distribution, and reproduction in any medium, provided the original work is properly cited.

The application of remote sensing images in water body recognition has become an effective method for ecological environment detection and evaluation, which has the disadvantages of low efficiency due to the existence of interpretation marks and rich interpretation experience in the current water body environment recognition, and overreliance on human experience. In this paper, the water body recognition method is applied to remote sensing images by combining the deep convolution generation network and the combined features, which has the advantage of high recognition accuracy. In the convolutional neural network, a five-layer convolutional neural network is used to construct a remote sensing water information extraction model, the transfer learning idea is introduced, and the densely connected feature fusion structure is added, so as to achieve the purposes of accelerating the convergence speed of the neural network, reducing the requirements of the neural network on the scale of training data, and reducing the loss of spatial hierarchical information and small object information. Compared with SVM, DBN, and CNN models, the experimental results show that the recognition accuracy of the proposed method is as high as 95.69% under the constraint of scale window, which has a wide range of application scenarios and practical significance.

## 1. Introduction

Remote sensing technology is a technology that collects electromagnetic radiation information of ground objects and targets from artificial satellites, aircraft, or other aircraft and identifies the earth's environment and resources [1]. Real-time and efficient remote sensing data are obtained by means of remote sensing technology, and a series of work such as flood range extraction, disaster location, disaster information analysis, and disaster development trend evaluation are completed, providing data guarantee for remote sensing monitoring of flood disasters [2]. Satellite remote sensing is a sharp weapon for natural disaster monitoring, which plays an important role in natural disaster prediction, monitoring and early warning, risk assessment, decision-making and command, emergency rescue, recovery and reconstruction, etc. In recent years, UAV remote sensing technology has been widely used in disaster reduction and

relief work of natural disasters such as earthquakes, floods, and typhoons and has played an important role in pre-disaster early warning preparation, disaster monitoring and rescue, and post-disaster assessment and recovery. Compared with unmanned aerial vehicle remote sensing, the advantage of satellite remote sensing lies in the periodic revisit of satellites, which can continuously obtain post-disaster data. By making the time series analysis map of water body changes in disaster areas, the information of water body changes in disaster areas can be obtained, and the disaster situation can be analyzed. However, during the flood disaster, the affected areas are often cloudy, rainy, and other bad weather, and optical remote sensing satellites are greatly affected by the weather, so it is difficult to obtain high-quality optical remote sensing satellite images. At the same time, the revisit period of medium- and high-resolution observation satellites can reach several days to ten days. When floods suddenly occur, there may be a problem that there is no satellite

transit. Unmanned aerial vehicle (UAV) remote sensing has the advantages of fast response speed, strong maneuverability, and working under the cloud, which is more in line with the characteristics of high timeliness and accuracy of data acquisition in flood emergency relief. The rapid development of UAV remote sensing technology provides us with a reliable means to obtain real-time disaster information. The UAV flight platform is equipped with various sensors, which can accurately obtain the real-time image data of the disaster area. After interpretation and analysis, the disaster information of the width of the levee breach; the flooded area; the damage of buildings; the damage of roads in the disaster area, crops, and aquaculture; etc. can be extracted, providing important data support for the decision-making of disaster reduction and relief work.

With the development of artificial intelligence and machine learning technology and with the help of artificial intelligence machine learning algorithm relying on remote sensing images, intelligent analysis, automatic extraction, and visual display of remote sensing data show the characteristics of high timeliness, low cost, more convenience, and more accuracy, which changes the disadvantages of traditional remote sensing data processing, such as long time-consuming and low efficiency and brings great changes to the application of massive remote sensing data [3]. Based on the deep learning semantic segmentation technology of remote sensing images [4], a neural network semantic segmentation model is constructed by using the deep learning method. By automatically learning and extracting the features of remote sensing images, end-to-end classification learning is carried out, and each pixel in the images is assigned to its own category label. Compared with traditional methods, the depth combination of remote sensing spatial information and model algorithm has made great progress in remote sensing image classification, object detection, image semantic segmentation, and other application directions [5].

Previously, we proposed a deep neural network for obtaining remote sensing images for reconstruction, but there are some problems, such as the deeper the network trains Vietnam; low resolution and low frequency information will be regarded as high frequency information [6]. Therefore, we propose a single-resolution superresolution algorithm based on gated convolution neural network (PGCNN), which is mainly composed of multiple residual blocks, each of which contains well-designed gated convolution units, which can provide weights to control the transmission of high and low frequency information, so the main network has more value for high frequency information processing. Convolution neural network is widely used in remote sensing field, but the core of remote sensing intelligent task is to solve the context information in images. Because the traditional architecture method is only to improve efficiency, so that the image size can be adjusted to a smaller resolution to simplify the data, which will make the information in the text lost. A learning framework of context information retention architecture for remote sensing scene classification is called CIPAL for short. It makes the most of the context information in RSIs and also intro-

duces channel compression to reduce memory and time, so there is more architecture space. Experiments show that CIPAL is more time-saving than similar architectures. On the other hand, it helps us understand that different types of representations are very important for RSI intelligent understanding [7].

With the rapid urbanization process, how to detect building information quickly and accurately is a hot research topic at present. There are a series of problems in traditional algorithms, such as poor semantic segmentation and rough edges [8]. At present, the improved U-Net-based deep convolution neural network uses end-to-end semantic segmentation and model fusion strategy, which makes the data set up to 70.4%. In the field of remote sensing image processing, there are often a large number of image data. Generally, superresolution methods are used to restore images to high resolution, but there are many parameters and large amount of calculation, which is not practical. Therefore, a feedback ghost residual dense network (FGRDN) is proposed. The convolution of residual dense blocks (RDBs) is replaced by ghost modules (GMs) in this network, which avoids parameter increase, converges parameters quickly, and improves network performance [9]. With the development of science and technology, UAV is no longer simply used for entertainment but has been used in various studies. We propose a water range estimation method based on UAV remote sensing data, which mainly uses sensors to collect and process data and obtain exact information to estimate water range. In the experiment, three kinds of sensors are selected and carried by UAV, and 6 water bodies are taken as data. Finally, several strategies for estimating water body range by using image processing tools are obtained. The results show that the thermal infrared orthogonal splicing is the best [10]. The difference of sensor type and product will affect the plane accuracy of water body range. The above research work has certain research significance for the recognition and application of neural network in water images, which solves the application problems in different scenes and improves the safety of people's lives. However, this solution is studied under the traditional technology and algorithm, and its recognition accuracy and accuracy are low. When facing the specific scene application, the algorithm produces different effects. The convolutional neural network proposed in this paper is based on the traditional algorithm for water recognition and application in specific scenes and has good results from the application of this paper.

## 2. Remote Sensing Water Body Recognition Based on Convolution Neural Network

*2.1. Overview of Convolution Neural Networks.* Convolution neural network was proposed by Fukushima University in 1988 and widely used in the field of machine learning [11] ferent from SDAE model; convolution neural network model adopts supervised learning. Firstly, the higher-order features of water body are studied in convolution layer and pool layer, and then, BP algorithm is used to optimize the whole neural network in the whole connection layer to minimize the error [12, 13]. The convolutional neural network is

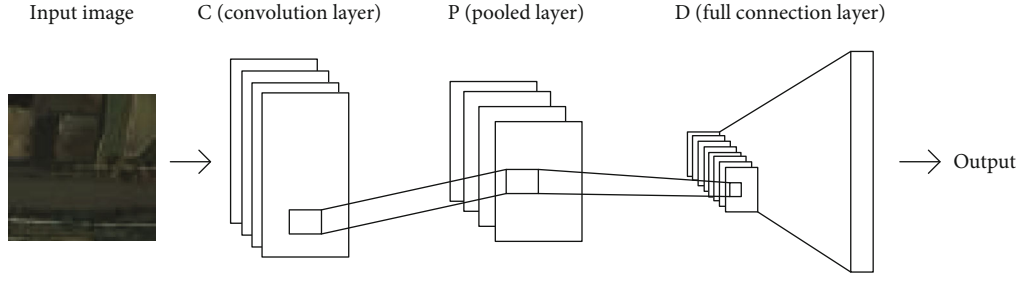


FIGURE 1: Schematic diagram of CNN network structure.

constructed by imitating the biological visual perception mechanism and can perform supervised learning and unsupervised learning. The convolutional kernel parameter sharing in the hidden layer and the sparsity of interlayer connections enable the convolutional neural network to learn lattice features, such as pixels and audio, with a small amount of computation, a stable effect, and no additional feature engineering requirements for data.

The specific step of training convolution neural network is to randomly select a sample  $(X, Y)$  from all alternative training samples, take  $X$  as the input of the network, transmit it to the output layer through subsampling and some convolution, and calculate the corresponding actual output value [14]. The calculated actual output value  $O$  is compared with the expected output value  $Y$ , and an error value is calculated. According to the principle of minimum error value, the weight matrix is adjusted in the opposite direction of each layer until the actual error reaches the expected error.

$$E_p = \frac{1}{2} \sum_j (y_{pj} - o_{pj})^2. \quad (1)$$

The network diagram of convolution neural network (CNN) extracting features from remote sensing images is shown in Figure 1.

For training convolution neural network, the specific transformation and fine-tuning process are as follows:

- (1) See Equation (2) for the calculation formula of feature learning and classifier:

$$\begin{cases} X = f(x, \omega, b), \omega \in R^w, b \in R^b, \\ Y = \text{softmax}(X, \theta). \end{cases} \quad (2)$$

- (2) The objective function is optimized by Formula (3)

$$\min_{\theta} J(\omega, b, \theta) = -\frac{1}{N} \sum_{m=1} \sum_{n=0} \log(Y_m(n)) + \alpha R(\omega) + \beta R(b), \quad (3)$$

where  $\alpha$  and  $\beta$  are the attenuation coefficients of weight and bias, respectively.

**2.2. Joint Feature Extraction.** By analyzing the spectral features, texture features, and spatial geometric features of domain water, the following features are selected as the input data of convolution neural network:

- (1) *Single Band Threshold.* By detecting the brightness value of short infrared band, we can sense the slight change of surface soil water content within a certain threshold range, which can be used to distinguish water from other surface objects. Formula (4) is defined as follows:

$$\text{Band5} > T. \quad (4)$$

- (2) NDWI is usually used to calculate the area coverage of water bodies in an area. Because of the close relationship between the water body and the surface vegetation, even in places with abundant water resources, the vegetation is very lush. Therefore, the use of NDWI increases the spectral differences between water and vegetation. Formula (5) is defined as follows:

$$\text{NDWI} = \frac{\text{NIR} - \text{Green}}{\text{NIR} + \text{Green}}. \quad (5)$$

- (3) *Multiband Spectral Relationship Method.* Multiband spectral relation method is to effectively combine the four bands in remote sensing images, enhance the difference between water information and shadow, and accurately and quickly eliminate shadow information caused by external environment or other factors. Formula (6) is defined as follows:

$$(\text{Band2} + \text{Band3}) - (\text{Band4} + \text{Band5}) > 0. \quad (6)$$

- (4) *Improved Normalized Water Body Index.* It uses logical expressions related to midinfrared band (MIR) and green belt structure to enhance the contrast

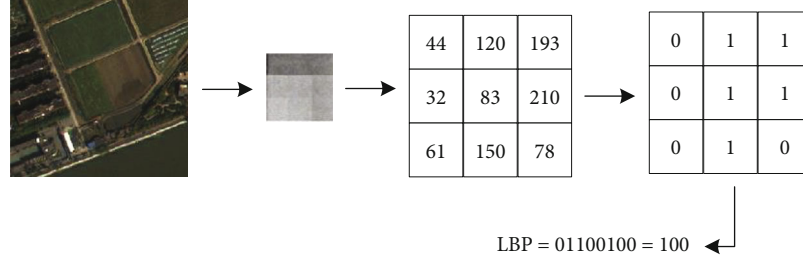


FIGURE 2: Schematic diagram of LBP.

TABLE 1: Comparison table of network training parameters.

Activation function of convolution neural network	Error	Max iteration
Input layer		
Output layer		
RBF = 0.4	CNN	0.012
		250

between water body and surface buildings and reduce the confusion influence on remote sensing water body recognition. Formula (7) is defined as follows:

$$\text{MNDWI} = \frac{\text{MIR} - \text{Green}}{\text{MIR} + \text{Green}}. \quad (7)$$

- (5) *Normalized Building Index*. Using NDBI of short infrared band and midinfrared band, the corresponding formula is constructed to eliminate the building information in water body of remote sensing image. Formula (8) is defined as follows:

$$\text{NDBI} = \frac{\text{MIR} - \text{NIR}}{\text{MIR} + \text{NIR}}. \quad (8)$$

- (6) *Histogram Features in Spatial Information*. Image histogram features extracted by using gray value and direction change of local texture of remote sensing image. The specific calculation process of histogram features in spatial information is as follows:

Assuming a point  $c$  centered on an arbitrary number of pixels  $(x, y)$  in a local area of the remotely sensed image, Formula (9) represents a concrete display of eight pixel points and textures adjacent to the window  $3 \times 3$ :

$$N(C_1 - C_i, \dots, C_8 - C_i). \quad (9)$$

Other pixels in the window are binarized, that is, "0" and "1." The calculation formula is shown as follows:

$$N \approx (S(C_1 - C_i, \dots, C_8 - C_i)), \quad (10)$$

where  $S$  stands for:

$$S(X) = \begin{cases} 1, & X > 0, \\ 0, & X \leq 0. \end{cases} \quad (11)$$

When the 8-bit binary number is obtained and the weights of pixels at different positions are determined according to (12), the LBP value of the window is obtained, as shown as follows:

$$\text{LBP}(X_i, Y_i) = \sum_{j=1}^8 S(C_j - C_i) 2^j, j = 1, \dots, 8. \quad (12)$$

The LBP value of the center pixel is shown in Figure 2.

**2.3. Training Sample Selection.** The quality of selected training samples not only has an important impact on the accuracy of remote sensing water body recognition [15, 16]. In this paper, the following methods are designed, and the spectral characteristics of water bodies in the experiment are automatically selected.

**2.3.1. "Matrix Roulette" Training Sample Selection Method.** Assuming that the total number of training samples is  $a$ , the remote sensing image of the whole study area is regarded as a segmented  $i * j$  "matrix round" to ensure that the selected samples are randomly distributed in the image of the whole study area, and samples  $A/i * j$  are randomly selected in each rectangular area so that the selected training samples cover the image of the whole study area.

**2.3.2. Selection of Training Samples for "GNDWI" Index.** Aiming at the difficulty and low automation of traditional sample selection, a threshold segmentation method of remote sensing image based on multiband spectral relationship is proposed. The specific steps of the algorithm are as follows.

*Step 1.* Calculate the GNDWI index value of the image pixels in the study area, set the appropriate threshold value, and preliminarily segment the remote sensing image. See Formula (13) for the specific calculation formula:

$$\text{GNDWI} = \frac{\text{NDWI} - \text{NDWI}^c}{\lambda}. \quad (13)$$

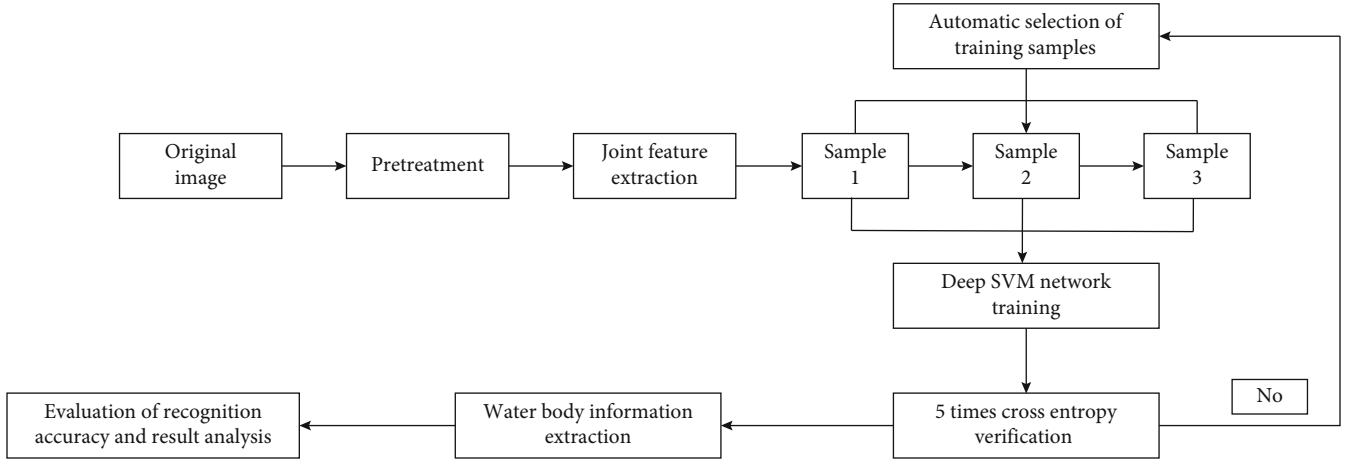



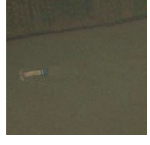

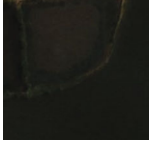


FIGURE 3: Specific flow chart of water body information extraction.

TABLE 2: Detailed information table of study area.

Image serial number	Study area	Imaging time	Strip number	Climate
1	Shanxi	June 2021	34/126	Drought
2	Xinjiang	June 2021	29/146	Drought
3	Gansu Province	August 2020	37/129	Damp

TABLE 3: Image data of some experimental samples.

Image serial number	Name	Height * width	Sum of pixels	Experimental sample
1	SX_1	227*250	56750	
2	SX_2	250*302	75500	
3	GS_1	400*302	120800	
4	GS_2	200*150	30000	
5	XJ_1	302*302	91204	
6	XJ_2	500*158	79000	

SX: Shanxi; XJ: Xinjiang; GS: Gansu.

*Step 2.* Use multiband spectral relationship method to calculate the eigenvalues of all pixels in the study area. Set a reasonable defect value to segment the image twice to obtain more accurate water information.

*Step 3.* Use (14) to select training samples.

$$A = \sum_{i,j} (\theta_i * A_{\text{water}} + \theta_j * A_{\text{other}}), \quad (14)$$

where  $\theta_i$  and  $\theta_j$ , respectively, represent the proportion of water samples and nonwater samples in the total samples in the whole study area. The setting of its value is obtained by experimental test.

**2.3.3. Feature Selection of Spatial Features.** In order to make full use of the spatial structure information between adjacent pixels in the image, we calculate the average value of all nearby pixels in the  $n * n$  window and help to extract new special data as the input of the model.

**2.4. Modeling.** Firstly, as the input of the neural network convolving the obtained new feature set (32 dimensions), the number of input nodes of the model is 32 (nodes correspond to the feature dimension one by one), and then  $Y$  is "0" and "1," that is, water body and nonwater body. The number of nodal neurons in the implicit layer of the model is obtained as follows:

$$S = \sqrt{i+j} + \lambda. \quad (15)$$

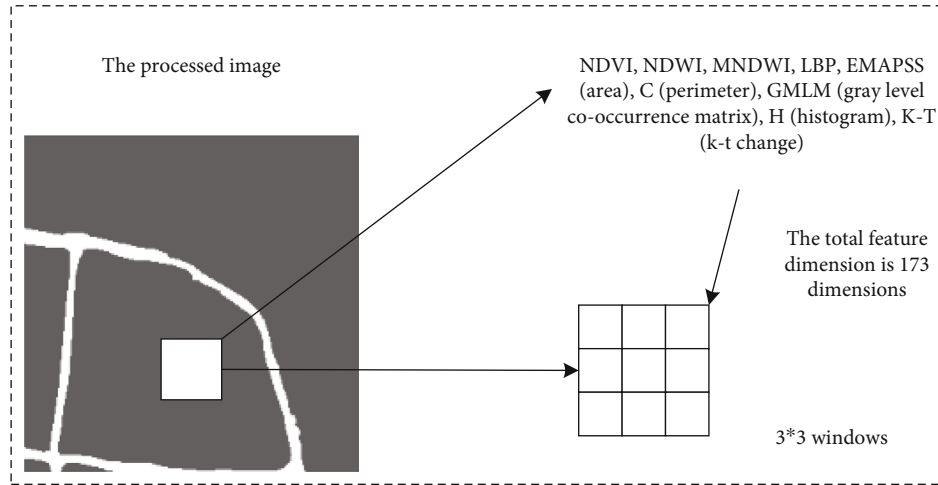


FIGURE 4: Construction of new feature matrix.

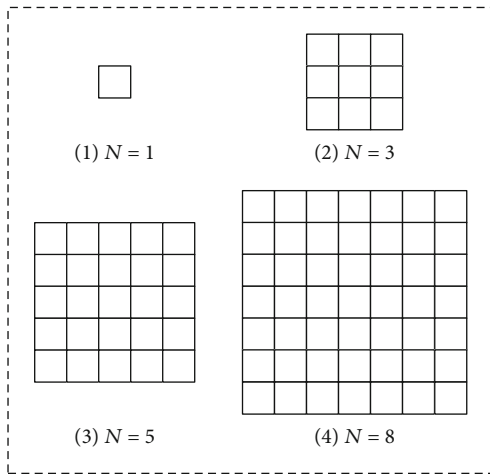


FIGURE 5: Joint feature calculation process of windows with different scales, where  $N$  represents windows with different proportions.

Through experimental tests, the final parameters are  $i = 32$ ,  $j = 2$ , and  $\lambda = 12$ ; the number of hidden neurons in the two layers is 18 and 16, respectively, and the free kernel function RBF is 0.4, as shown in Table 1.

The convolution neural network model is initialized by the abovementioned network parameter comparison table, and a remote sensing water information extraction model is constructed, which consists of 32 input units, 18 and 16 hidden layer units, 1 convolution neural network unit, and 2 output units. The specific flow chart is shown in Figure 3.

Firstly, the algorithm is used to extract features and select samples from the image of the study area, and test samples and training samples are obtained, respectively. Then, in order to solve the overfitting phenomenon and enhance the model, five adjoint cross entropy principles are used to test the generalization ability of samples, so as to realize faster convergence of convolution neural network.

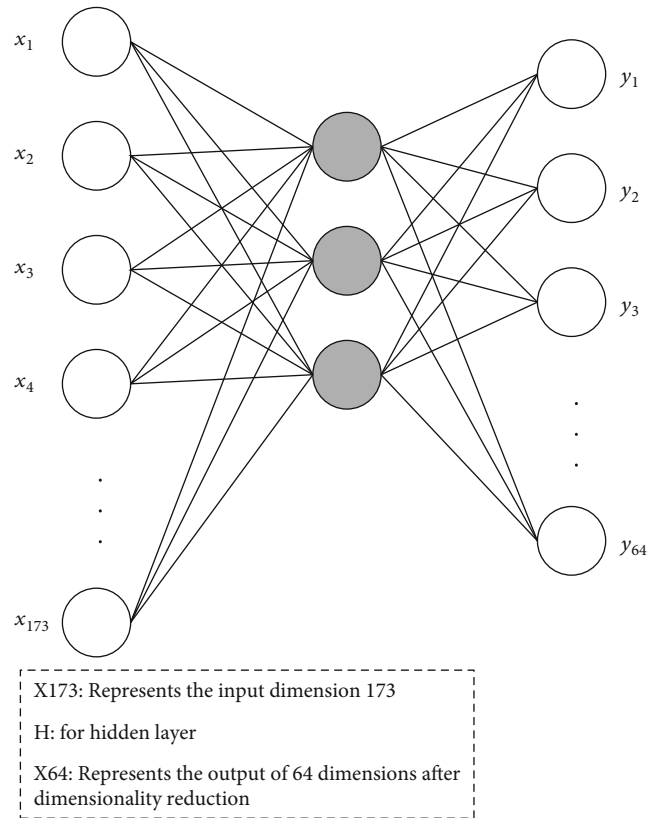


FIGURE 6: Dimension reduction schematic diagram.

### 3. Combining Depth Convolution Generation Network and Joint Features for Water Body Recognition

3.1. Introduction of Study Area and Experimental Data. In this paper, the details of the selected research fields are shown in Table 2.

Where the study area selected by Xinjiang is centered on Yilichuan Basin, Gansu is the coastal waters of Jialing River

TABLE 4: Initialization settings of water body identification model parameters.

Number of input layer nodes (feature dimension)	64	
Number of output layer nodes	2 (water and nonwater)	
Generate model ( $G$ )	Learning rate	0.005
	Momentum	0.9
Discriminant model ( $D$ )	Learning rate	0.005
	Momentum	0.9
Number of iterations	1000	
Activation function	tanh	
Classification function	SoftMax	
Convolution kernel size	5	
Pool layer filter size	2	
Number of neurons in full connection layer	1024	

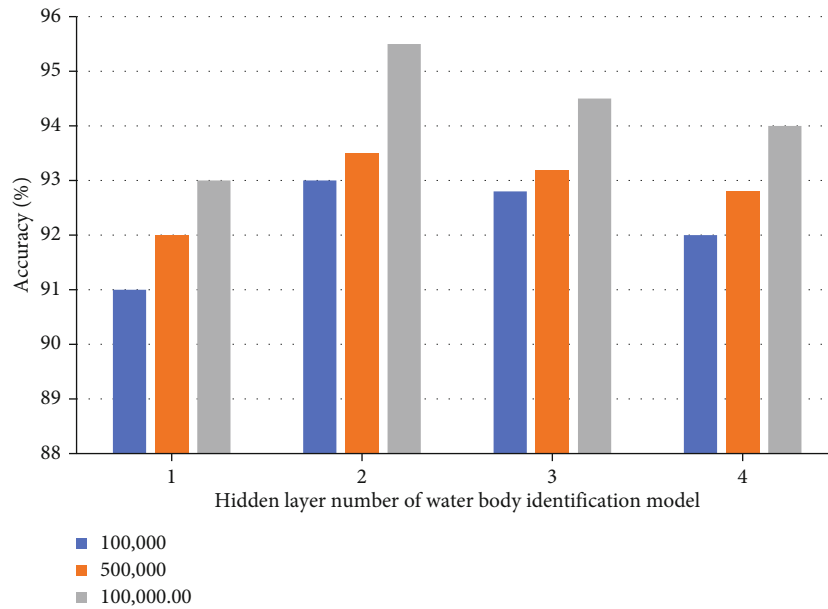


FIGURE 7: Influence of hidden layer number in water body identification model on experimental results.

TABLE 5: Comparison table of experimental results.

Accuracy%, layers	1	2	3	4
100,000	91.02	93.09	92.78	91.89
500,000	92.1	93.65	93.32	92.79
100,000.00	93.26	95.69	94.39	93.98

TABLE 6: Comparison of experimental results.

Accuracy%, model	SVM	DBN	CNN	DCGAN
100,000	92.13	94.19	94.34	93.09
500,000	93.64	94.76	94.88	93.65
100,000.00	94.53	95.39	95.31	95.69

in southern Gansu, and Shanxi is Luliang. Selecting the above three areas as the study area, the recognition generalization ability of the proposed model and the same water distribution situation in different areas are verified.

**3.2. Remote Sensing Image Preprocessing.** Before the experiment, the remote sensing images of the three regions were digitized to improve the image quality and reduce the impact on the accuracy of the water body recognition model.

Experiments were carried out on four images, and each image had different clipping sizes. Finally, some images are randomly selected from the images of each region as training samples and the rest as test samples. Some experimental samples are shown in Table 3.

**3.3. Spatial Joint Feature Extraction.** Remote sensing images are composed of multiple bands, and the spectral reflectance of water in different bands is not near G phase. Therefore, it is of great significance to extract spectral features of water

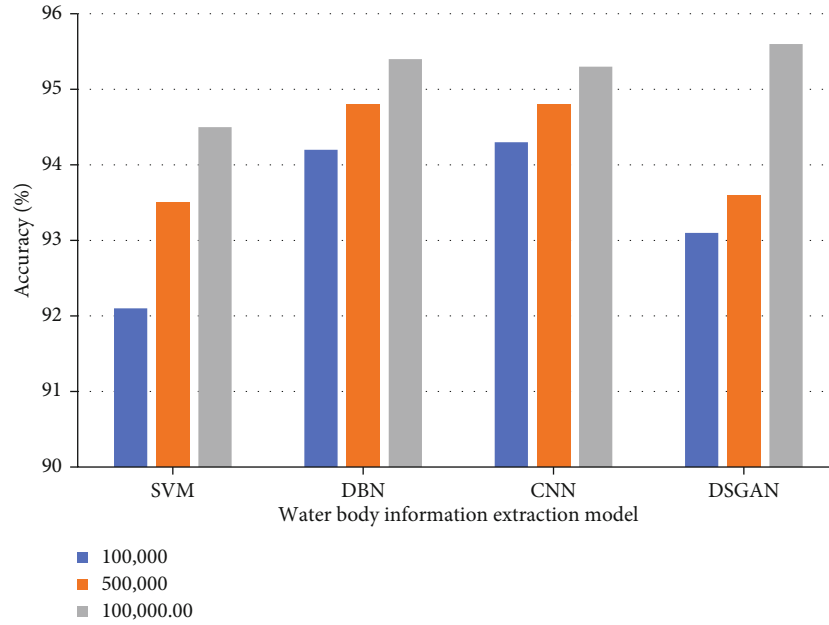


FIGURE 8: Experimental comparison results.

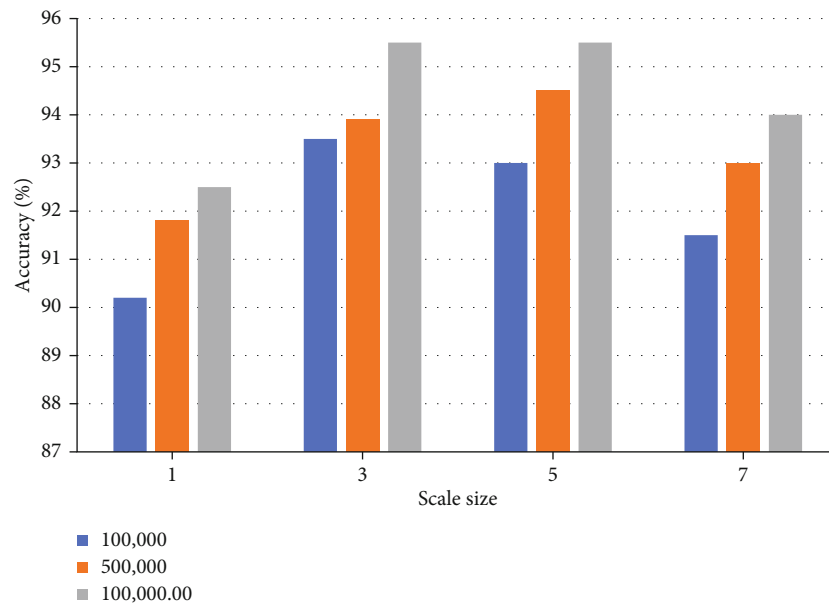


FIGURE 9: Experimental results.

bodies. In order to better understand and grasp the dynamic characteristics of water body, researchers at home and abroad have put forward many methods to extract spectral characteristics of water body (such as water index method) [17].

However, only using spectral features cannot fully characterize the fine local water information. Therefore, there are many methods to extract spatial information from remote sensing images based on mathematical models [18, 19].

Figure 4 shows the new feature matrix construction process and the relationship between each pixel and the corresponding matrix.

The 3\*3 window represents the constraint window size; that is, the scale size is 3\*3. When the color window is too large, the detailed information of the water body is easily lost. If the color window is too small, the water body information in the remote sensing image cannot be well represented. Therefore, the experimental results show that the window size of the final selected scale is 3\*3; that is,  $N = 3$ .

*3.4. Constraint Algorithm for Joint Features.* The basic steps of the constraint algorithm are as follows:



TABLE 7: Initialization settings of model parameters.

Number of input layer nodes	64
Number of nodes in output layer	2 (water and nonwater)
Hidden layer number of generation model and discrimination model	They are all 2 floors
The number of hidden layer nodes, respectively	128 and 256
Fully connected layer	1024

TABLE 8: Comparison of experimental results.

Accuracy%, scale	1	3	5	7
100,000	90.39	93.09	93.19	91.41
500,000	91.71	93.65	94.35	92.99
100,000.00	92.43	95.69	95.03	93.84

- (1) Each remote sensing image is a pixel point group. In the object image, any pixel point is taken as the object pixel point, and  $N * N$  of the central pixel point is taken as the pixel point in the reference window area
- (2) Setting the pixel points in the  $N * N$  window of the pixel points to be identified, respectively, obtaining the spectral and spatial combined characteristics of each pixel point in the scale window
- (3) Based on the given spectral and spatial coupling, including the unique constraint algorithm and formula, the sum of pixels in the region window is calculated
- (4) Finally, after obtaining the sum of all the pixels in the region window, the average value of all the pixels is calculated
- (5) As a new feature set, the size of the scale window can be controlled by adjusting the size of  $N$  using the average value of the identified pixel points. Figure 5 shows the calculation process of common features in different scale windows

In order to improve the accuracy in the recognition model of spectral and spatial coupling characteristics [20, 21], the scale window with the size of  $N = 3$  is finally selected not only to preserve the correlation between aberrations but also to preserve the detailed features of underwater information in remote images as much as possible. However, due to the high dimension of coupling characteristics extracted by spectral and spatial constraint algorithms and the great difficulties in the operation of the model [22, 23], this paper maps the high-order element characteristics from the encoder to the low-dimensional space of the nonlinear unary scheme to test the smooth operation of the model. As shown in Figure 6, a schematic process of dimension decline is shown.

#### 4. Experimental Results and Analysis

Using the powerful self-learning ability and high-order feature mining ability of deep learning algorithm, a water infor-

mation extraction model based on deep deconvolution game generation network and combined features is established. Visual Studio 2021 and Anaconda 3 are used to build an experimental simulation platform, and the effective features of water signal sum in remote sensing images are extracted by spectral and spatial coupling feature constraint algorithm [24]. The overall performance of the proposed water information extraction model is tested by experiments.

In the water information extraction model, the initial settings of the number of layers and nodes are shown in Table 4.

*4.1. Influence of the Number of Hidden Layers on the Experimental Results of Water Information Extraction Model.* When depth deconvolution competes with generation model, the change of hidden layer between generation model and discrimination model will also have a certain impact on water identification model. Select three different sets of experimental data in the above table to test the performance of the model, and change the number of hidden layers to find the best number of hidden layers of the model. The specific experimental results are shown in Figure 7.

Specific experimental results are compared as shown in Table 5.

As can be seen from Table 5 and Figure 7, if the amount of image data is fixed, the recognition accuracy may increase in advance and decrease as the number of implicit layers of the water information extraction model increases. As can be seen from the above figure, when the number of hidden layers is 2, the accuracy is the highest, which is opposite to the water body recognition accuracy of the network model generated by depth convolution proposed in this paper. On the other hand, if the amount of training data reaches 800,000 and the amount of test data reaches 200,000, the recognition accuracy of the water body recognition model reaches 95.69%. In order to obtain better water information extraction results, the hidden layer of the discriminant model in the generation model and the resistance model is set to two layers, and the parameters of other models are shown in Table 6.

*4.2. Comparison with Traditional Machine Learning Models.* In order to test the overall performance of the network water information extraction model and the proposed depth convolution generation, a traditional machine learning algorithm is extracted and compared with the proposed model. Similarly, we optimize the parameters of the comparative machine learning model in order to accurately evaluate the performance of the proposed water recognition model. The comparison of specific experimental results is shown in Figure 8.

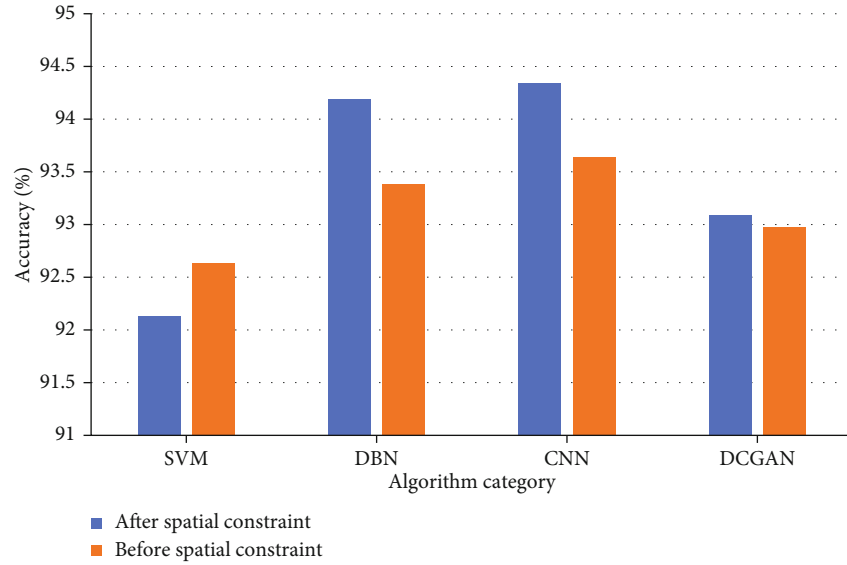


FIGURE 10: Model-comparison of experimental results before and after spatial constraint of 100,000.

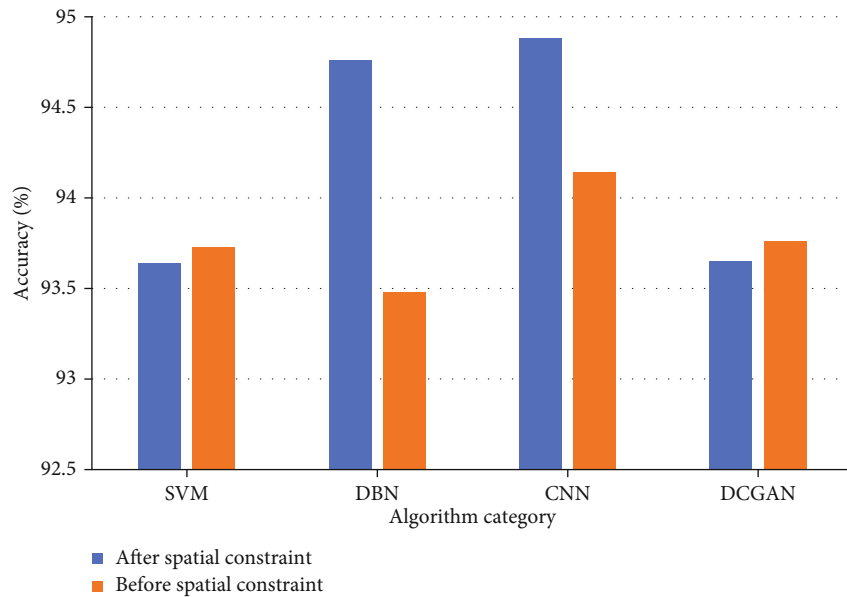


FIGURE 11: Model-comparison of experimental results before and after spatial constraint of 500,000.

Specific experimental results are compared as shown in Table 6.

See Figure 8 and Table 6. It can be seen from the figures and tables that with the increase of remote sensing image data, the accuracy of all water body recognition models is steadily improving. With the increase of input data, these machine learning models can learn more effective water feature information from image data, so the accuracy of water recognition can be improved with the increase of data.

*4.3. Influence of the Size of Constraint Scale Window on Water Body Recognition Results.* In order to find the best constraint window, this summary uses several scaled win-

dows in Figure 9 to test the proposed water body identification model. If the amount of input data of the remote sensing image is constant, the features in the case of window sizes  $n = 3, 5,$  and  $7$  are spatially limited. The basic initialization parameter settings of the model are shown in Table 7.

In the constraint algorithm of spectral and spatial coupling characteristics, the size of scale window has an important influence on the final recognition effect of water body recognition model. Therefore, pixels of target objects in different zoom window areas can be identified. Then, choose the best  $n$  and compare it with the experimental results. The experimental pair is shown in Figure 9.

The comparison table of specific experimental results is shown in Table 8.

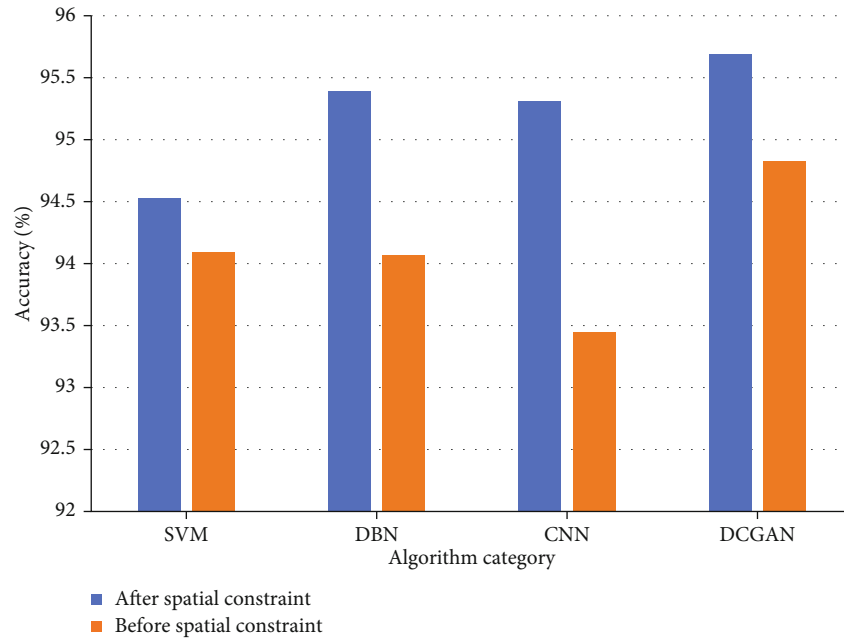


FIGURE 12: Model-comparison of experimental results before and after spatial constraint of 1 million.

As can be seen from Table 8 and Figure 9, when the amount of input data is constant, with the increase of scale window  $N$ , depth convolution occurs, which reduces the recognition accuracy of the water body recognition model. This means that the closer the recognition pixel is, the greater the impact on the recognition pixel. The farther the distance, the smaller the impact. Experimental results show that when the scale window is  $n=3$ , the accuracy of water body recognition model is high. Therefore, the extraction ratio window of spectral and spatial coupling features is set to 3.

**4.4. Test the Effectiveness of Spectral and Spatial Joint Feature Constraint Algorithm for Water Body Information Extraction.** By testing the spectral and spatial constraint algorithms, we verify the effectiveness of the whole model. When the scale window  $n$  is set to 3, an average of all pixels in the  $n*n$  window is obtained to combine the reconstructed new features with the input data of the water body recognition model. The specific experimental results are shown in Figures 10–12.

As can be seen from Figures 10–12, if the water body recognition model is trained using the constrained common features, the water body recognition model obtains a better recognition effect. Because of the coupling characteristics of spectrum and space, the constraint algorithm not only eliminates the spatial correlation between adjacent aberrations in remote sensing images but also reduces the interference of other aberrations in adjacent areas on recognition aberrations. Figures 10–12 show the different amounts of data, respectively. When the amount of input data reaches 1 million, whether there are spatial constraints or not, the recognition effect of water body recognition model based on depth convolution is better than other traditional machine learning algorithms.

## 5. Conclusion

Obtaining more accurate and less noisy water information from remote sensing images is the key to water body recognition. By introducing the concept of distributed parallel computing and based on deep learning mode, the correctness, automation, and running speed of extracting models from water information are improved to a certain extent. However, with the geometric growth of remote sensing image data, how to obtain more and more accurate marker data for training water body recognition model is a challenge. To solve the above problems, this paper constructs a water body information extraction model with stable spectral and spatial coupling features by using different feature knowledge such as spectrum, texture, shape, and spatial geometry and identifies water bodies in remote sensing images through depth learning model. Considering the constant correlation between adjacent pixels in remote sensing images, we propose a spatial constraint algorithm with spectral and spatial coupling features to extract new common features and use the new feature set as the input solution of the depth learning model to train the model, so as to realize the correct extraction of water information. Experimental results show that the traditional deep learning water recognition model is superior to shallow support vector machine (SVM) network in learning ability and feature extraction ability. The water body recognition model proposed in this paper has good representativeness in feature learning and image data processing of generation model and discrimination model and has higher recognition effect than traditional beam learning model.

## Data Availability

The experimental data used to support the findings of this study are available from the corresponding author upon request.

## Conflicts of Interest

The authors declared that they have no conflicts of interest regarding this work.

## Acknowledgments

This work was sponsored in part by the Industry University Cooperation Collaborative Education Project (202102453006).

## References

- [1] C. Haijian, "Application and development prospect of remote sensing technology in environmental monitoring," *China New Technology and New Products*, vol. 13, pp. 6-7, 2011.
- [2] J. Zhang, L. Yahui, Y. Wenju, L. Gao, D. Zhu, and J. Yang, "Research progress analysis of remote sensing monitoring of land remediation," *Journal of Agricultural Machinery*, vol. 50, no. 1, pp. 1-22, 2019.
- [3] Editorial Department of this Journal, W. Zhiqiang, H. Xiaochun et al., "Academic writing conference on the impact of artificial intelligence on urban planning," *Journal of Urban Planning*, vol. 5, pp. 1-10, 2018.
- [4] S. Wang, X. Mu, D. Yang, H. He, and P. Zhao, "Road extraction from remote sensing images using the inner convolution integrated encoder-decoder network and directional conditional random fields," *Remote Sensing*, vol. 13, no. 3, p. 465, 2021.
- [5] Y. Zhang, D. Zhang, J. Duan, and T. Hu, "Mapping of intrusive complex on a small scale using multi-source remote sensing images," *International Journal of Geo-Information*, vol. 9, no. 9, p. 543, 2020.
- [6] Y. Peng, X. Wang, J. Zhang, and S. Liu, "Pre-training of gated convolution neural network for remote sensing image super-resolution," *IET Image Processing*, vol. 15, no. 5, pp. 1179-1188, 2021.
- [7] J. Chen, H. Huang, J. Peng et al., "TEMDnet: a novel deep denoising network for transient electromagnetic signal with signal-to-image transformation," *IEEE Transactions on Geoscience and Remote Sensing*, vol. 60, no. 99, pp. 1-18, 2021.
- [8] L. X. Weiyang, "The application of deep convolution neural network to building extraction in remote sensing images," *World Scientific Research Journal*, vol. 6, no. 3, pp. 136-144, 2020.
- [9] J. Wang, Y. Wu, L. Wang, L. Wang, O. Alfarraj, and A. Tolba, "Lightweight feedback convolution neural network for remote sensing images super-resolution," *IEEE Access*, vol. 9, pp. 15992-16003, 2021.
- [10] P. Tymków, G. Józaków, A. Walicka, M. Karpina, and A. Borkowski, "Identification of water body extent based on remote sensing data collected with unmanned aerial vehicle," *Water*, vol. 11, no. 2, p. 338, 2019.
- [11] L. Lou and Y. Li, "A seismic image denoising method based on kernel-prediction CNN architecture," *International Journal on Artificial Intelligence Tools*, vol. 29, no. 7n08, p. 2040012, 2020.
- [12] W. Xia, Y. Wang, R. Liu, and S. Wang, "Research on flow and pressure prediction of urban water supply pipeline network based on GA-BP algorithm," *Journal of Physics Conference Series*, vol. 1792, no. 1, p. 012045, 2021.
- [13] W. Lu, C. Ma, and P. Li, "Research on sample selection of urban rail transit passenger flow forecasting based on SCBP algorithm," *IEEE Access*, vol. 8, no. 99, pp. 89425-89438, 2020.
- [14] X. M. Li, Y. Ma, Z. H. Leng, J. Zhang, and X. X. Lu, "High-accuracy remote sensing water depth retrieval for coral islands and reefs based on LSTM neural network," *Journal of Coastal Research*, vol. 102, no. sp1, pp. 21-32, 2020.
- [15] N. Karasiak, J. F. Dejoux, C. Monteil, and D. Sheeren, "Spatial dependence between training and test sets: another pitfall of classification accuracy assessment in remote sensing," *Machine Learning*, pp. 1-25, 2021.
- [16] J. Zhang and Y. Feng, "Advanced Chinese character detection for natural scene based on EAST," *Journal of Physics Conference Series*, vol. 1550, no. 3, p. 032050, 2020.
- [17] B. Fha, Y. Ying, and C. Tf, "Automatic extraction of impervious surfaces from high resolution remote sensing images based on deep learning," *Journal of Visual Communication and Image Representation*, vol. 58, pp. 453-461, 2019.
- [18] A. Denmukhammadiev, A. Paradaev, M. Begmatov, I. Abdirakhmonov, and M.'. Akhmedov, "Physicomathematical models of seeds and errors in calculating the volume of an electro terminator filled with seeds," *E3S Web of Conferences*, vol. 264, no. 6, p. 01053, 2021.
- [19] S. K. Govindarajan, A. Kumar, and A. Mishra, "Fluid flow through shale gas reservoirs: simplified conceptual and mathematical models," *Petroleum and Coal*, vol. 62, no. 3, pp. 776-791, 2020.
- [20] G. Yang, Y. Lin, and P. Bhattacharya, "A driver fatigue recognition model based on information fusion and dynamic Bayesian network," *Information Sciences*, vol. 180, no. 10, pp. 1942-1954, 2010.
- [21] A. K. Pavlou, N. Magan, D. Sharp, J. Brown, H. Barr, and A. P. F. Turner, "An intelligent rapid odour recognition model in discrimination of *Helicobacter pylori* and other gastroesophageal isolates in vitro [J]," *Biosensors & Bioelectronics*, vol. 15, no. 7-8, pp. 333-342, 2000.
- [22] J. Wang, J. Dong, and Y. Tan, "Role mining algorithms satisfied the permission cardinality constraint," *International Journal of Network Security*, vol. 22, no. 3, pp. 373-382, 2020.
- [23] K. M. Ting, Y. Zhu, M. Carman, Y. Zhu, T. Washio, and Z. H. Zhou, "Lowest probability mass neighbour algorithms: relaxing the metric constraint in distance-based neighbourhood algorithms," *Machine Learning*, vol. 108, no. 2, pp. 331-376, 2019.
- [24] J. Gabela, A. Kealy, M. Hedley, and B. Moran, "Case study of Bayesian RAIM algorithm integrated with spatial feature constraint and fault detection and exclusion algorithms for multi-sensor positioning," *Navigation*, vol. 68, no. 2, pp. 333-351, 2021.